RESEARCH ARTICLE

Zinc Metal Anode

Energy & Environmental Materials WILEY

Critical Factors Dictating Reversibility of the Zinc Metal Anode

Lin Ma, Marshall A. Schroeder, Travis P. Pollard, Oleg Borodin, Michael S. Ding, Ruimin Sun, Longsheng Cao, Janet Ho, David R. Baker, Chunsheng Wang, and Kang Xu**

With high energy density and improved safety, rechargeable battery chemistries with a zinc (Zn) metal anode offer promising and sustainable alternatives to those based on lithium metal or lithium-ion intercalation/alloying anode materials; however, the poor electrochemical reversibility of Zn plating/stripping, induced by parasitic reactions with both aqueous and non-aqueous electrolytes, presently limits the practical appeal of these systems. Although recent efforts in rechargeable Zn metal batteries (RZMBs) have achieved certain advancements in Zn metal reversibility, as quantified by the Coulombic efficiency (CE), a standard protocol for CE has not been established, and results across chemistries and systems are often conflicting. More importantly, there is still an insufficient understanding regarding the critical factors dictating Zn reversibility. In this work, a rigorous, established protocol for determining CE of lithium metal anodes is transplanted to the Zn chemistry and is used for systematically examining how a series of factors including current collector chemistry, current density, temperature, and the upper voltage limit during stripping affect the measured reversibility of different Zn electrolytes. With support from density functional theory calculations, this standardized Zn CE protocol is then leveraged to identify an important correlation between electrolyte solvation strength toward Zn^{2+} and the measured Zn CE in the corresponding electrolyte, providing new guidance for future development and evaluation of Zn electrolytes.

1. Introduction

Regarded as a potential alternative to Li-based battery anode materials, the Zn metal anode offers a high volumetric capacity (5854 mAh cm^{-3}),[1] relative abundance and widespread distribution in the earth's crust,[2,3] and a low plating/stripping potential that can be accommodated in aqueous electrolytes.[4–7] However, poor cycling efficiency and dendrite formation stemming from parasitic reactions between the Zn metal and the electrolyte currently impede the practical deployment of a rechargeable Zn metal battery (RZMB).[8,9] This impediment has spurred significant research effort toward electrolyte development for RZMBs.

Traditional alkaline electrolytes (e.g., 6 M KOH) have been widely studied[10–12] but still suffer from substantial impedance and limited reversibility[4] as a result of byproducts generated during cycling (e.g., ZnO and zincates). Advanced Zn anode architectures (e.g., Zn sponge,[13,14] backside-plating configuration[15]) have achieved some success in circumventing these limitations of alkaline electrolytes, extending full cell lifetime and with reduced self-discharge. Other recent efforts achieved improvements in Zn reversibility with mildly acidic aqueous electrolytes based on the Zn salts of superacids, including zinc sulfate ($ZnSO_4$),[16–18] zinc bis(trifluoromethylsulfonyl)imide ($Zn(TFSI)_2$),[19,20] and zinc trifluoromethanesulfonate ($Zn(OTf)_2$),[7,21] but further optimization is still needed to support a commercially viable RZMB. Researchers also applied the super concentration concept, showing that a high concentration of LiTFSI supporting salt suppressed water-induced parasitic reactions due to exclusion of H_2O from the Zn^{2+} solvation sheath[4]; however, these electrolytes exhibited increased viscosity and reduced conductivity as a result of the high salt concentration. Even with this progress in aqueous systems, each of these approaches (mildly acidic, alkaline, and super-concentrated) still suffers to varying extents from parasitic interactions with water, despite claimed CE values as high as 100%.[7] Alternatively, non-aqueous Zn electrolytes such as $Zn(TFSI)_2$ in propylene carbonate (PC)[22] or triethyl phosphate (TEP)[23] have shown great promise in supporting reversible Zn plating/stripping, with claimed Coulombic efficiencies (CEs) >99%. Based on these observations, published CE values provide extremely limited insight regarding the relative maturity of different electrolyte systems toward commercialization of an RZMB. The question is whether this is a limitation of the parameter itself, or a product of how CE is currently measured for Zn anodes.

CE is one of the primary parameters for quantifying the reversibility of an electrochemical system.[24–26] If measured under uniform, well-controlled conditions, the CE value can be an accurate predictor of cycle

Dr. L. Ma, Dr. M A. Schroeder, Dr. T P. Pollard, Dr. O. Borodin, Dr. M S. Ding, Dr. J. Ho, Dr. D R. Baker, Dr. K. Xu
Energy & Biotechnology Division, Sensors and Electron Devices Directorate, US Army Research Laboratory, 2800 Powder Mill Rd, Adelphi MD USA
E-mail: marshall.a.schroeder.civ@mail.mil
E-mail: conrad.k.xu.civ@mail.mil

Dr. R. Sun, Dr. L. Cao, Prof. C. Wang
Department of Chemical and Biomolecular Engineering, University of Maryland, Chem/Nuc building 4418 Stadium Drive, College Park 20742, MD USA

The ORCID identification number(s) for the author(s) of this article can be found under https://doi.org/10.1002/eem2.12077.

DOI: 10.1002/eem2.12077

life[26,27] and is useful for comparing the performance of different systems. However, the variability in cell setups, test protocols, and targeted parameters significantly limits the ability to draw effective performance comparisons both within and across these classes of electrolytes. In this work, we transplant an established Li CE "reservoir" method[26] to the Zn chemistry and clearly differentiate baseline and advanced non-aqueous and aqueous electrolytes under the same conditions as a demonstration. As an expansion to this study, we investigated the impact of several key factors including rate, temperature, metal substrate, and voltage cutoff during last stripping step on the Zn plating/stripping CE. Finally, with support from density functional theory (DFT) calculations, we propose a correlation between the measured CE (obtained using the same method) and ion/salt solvation free energy, providing new insight to guide further development of novel electrolytes for RZMBs.

2. Results and Discussion

Despite major fundamental differences between the Li and Zn chemistries, we found that published protocols for Li CE determination provide an excellent guide toward establishing an analogous protocol for Zn CE. In particular, we transplanted a galvanostatic technique proposed by Adams et al.[26] to measure Zn metal plating/stripping CE in both aqueous and non-aqueous electrolytes. In this method, we used a Cu|Zn cell setup with Cu as the working electrode and Zn as the counter electrode, Zn source, and reference. Substrate effects (lattice mismatch, alloying, interphase effects, etc.) are mitigated by an initial conditioning cycle, in which 5 mAh cm^{-2} of Zn is plated on and stripped from the Cu working electrode. Following this substrate conditioning step, a 5 mAh cm^{-2} "Zn reservoir" is subsequently plated on the Cu to provide a quantitatively limited and well-controlled source of Zn for accurate CE determination (Q_r). A fraction of this plated Zn reservoir (20%) is then cycled nine times at a fixed capacity of 1 mAh cm^{-2} (Q_c) at a rate of 0.5 mA cm^{-2}, followed by stripping to a preselected upper cutoff voltage (0.5 V vs Zn/Zn^{2+}), at which all removable Zn should be stripped, including the initial reservoir (Q_s). The CE is calculated based on Equation 1. In this protocol, we deliberately selected a moderate current density and a modest number of cycles to avoid anomalous CE measurements from effects such as Zn dendrite formation or excessive impedance growth.

Figure 1 shows a schematic of this method, including initial results for some of the most promising Zn electrolytes reported in the literature.[15,20,22,23] Surprisingly, some of the most common aqueous systems could not complete the protocol due to erratic voltage behaviors induced by parasitic reactions (Figure 1a,b and Figure S3a,b,f). These results yield no useful CE information, suggesting that these electrolytes may not be able to support Zn anode performance under realistic conditions (rates, capacities, loadings etc.). For the electrolytes that successfully completed the protocol, the non-aqueous systems show a clear advantage in CE over the tested aqueous electrolytes (Figure S3g). Interestingly, in the case of TEP-$Zn(TFSI)_2$ (Figure 1), note that despite completing the protocol, the overpotential growth with cycling and increasing concentration polarization during stripping indicates potential transport limitations for this electrolyte and a need for understanding CE dependence on the plating/stripping current.

Based on these results, we then selected a few electrolytes as exemplars for further study: 0.5 m $Zn(TFSI)_2$ in PC (A), 0.5 m $Zn(TFSI)_2$ in TEP (B), and 4 m $Zn(TFSI)_2$ in H_2O (C). Aside from rigorous testing of these electrolytes using the standard protocol, we also explored changes in CE as a function of current density, temperature, substrate metal chemistry, and upper cutoff voltage for stripping. **Figure 2** shows the results from these measurements, with error bars marking the difference between duplicate cells under the same conditions. All three electrolytes display substantial CE dependencies on the current density (Figure 2a), which can be attributed to the corresponding degrees of voltage polarization (Figure S4) and how much of the plated Zn that can be stripped before the working electrode potential reaches the preselected upper limit (0.5 V vs Zn/Zn^{2+}). High polarization (as in the example of electrolyte B at 2.5 mA cm^{-2}) significantly limits the recoverable capacity. Remarkably, the conductivities of electrolytes A and B are very close at room temperature (Figure S5), suggesting that other factors (e.g., Zn transference number, de-solvation energy, interfacial impedance [Figure S6], etc.) are the source for the difference in polarization. In contrast, aqueous electrolyte C displays much lower voltage polarization than the non-aqueous systems (below 0.1 V even at 2.5 mA cm^{-2} [Figure S4]), suggesting it may have superior stability; however, this electrolyte fails to survive in long-term cycling, as evidenced by its inability to complete a 9-cycle CE protocol at 0.25 mA cm^{-2} (Figure S7).

The impact of cycling temperature on the measured CE for the selected electrolytes at −10, 25 and 50 °C is shown in Figure 2b. The CE values for electrolyte C at −10 and 50 °C are missing because the electrolyte did not pass the initial galvanostatic protocol at these temperatures (Figure S8), despite its superior ionic conductivity (Figure S5). Conversely, the CEs of electrolytes A and B do not show an obvious temperature dependence except for a decrease in the CE of electrolyte B at −10 °C, which was attributed to a sudden increase in voltage polarization (Figure S9b) unrelated to any phase change or drop in ionic conductivity. The behaviors of electrolytes B and C suggest that cell polarization appears to be decoupled from the bulk ion conduction and more likely associated with interfacial/interphasial chemistries or morphology/roughness of the deposited Zn. We also investigated the effect of substrate material on the Zn plating/stripping reversibility, using Cu, Ti, and stainless steel (SS) electrodes, which are the most commonly used current collectors for the Zn chemistry (Figure 2c). From these experiments, the influence of these substrate metals on CE of non-aqueous electrolytes appears to be trivial as compared to the aqueous system, since electrolyte C is unable to finish the testing procedure on either SS or Ti current collectors (Figure S10). This difference is attributed to the varying degrees of hydrogen evolution activity of the metal substrates, which has been previously studied in Zn-based electrolytes.[28]

The upper cutoff voltage for the final stripping step was also varied between 0.25 and 0.5 V (vs Zn/Zn^{2+}) to study its effect on CE results. The CE changes in electrolytes A and C are minimal, but electrolyte B shows a dramatic dependence on the stripping cutoff voltage, which originates from the difference in voltage polarization during cycling (Figure S11). This presents a critical question: What is a realistic upper cutoff potential for stripping Zn metal from a non-Zn current collector (Cu, Ti, or SS) to gauge achievable performance in an "anode-free" full cell?

In an "anode-free" full cell, the highest potential a metal substrate (i.e., Cu vs Zn/Zn^{2+}) can reach depends on the substrate material, the cathode chemistry, and the discharge cutoff voltage of the cell. In the literature, this upper limit is often selected, somewhat arbitrarily, to be 0.5 V versus Zn. The underlying motivation for this specific value is based on the assumption that at this potential, all removable Zn has been stripped; however, this value may not actually be realistic or even achievable in a practical full cell. To accurately quantify this value in a

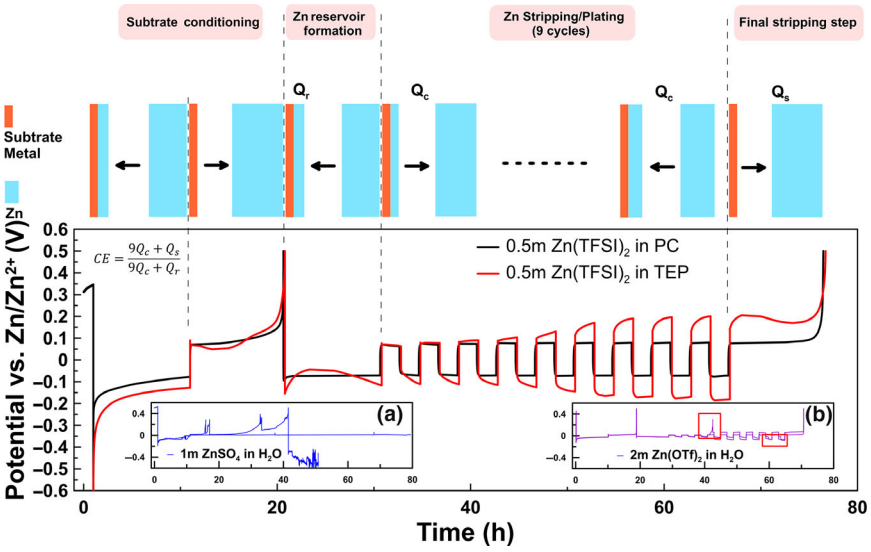

Figure 1. Proposed galvanostatic cycling protocol for evaluating Zn stripping/plating Coulombic efficiency (CE). The plots show the voltage versus time profile for Cu|Zn cells at 25 °C with different typical Zn electrolytes. CE results are summarized in Table S1.

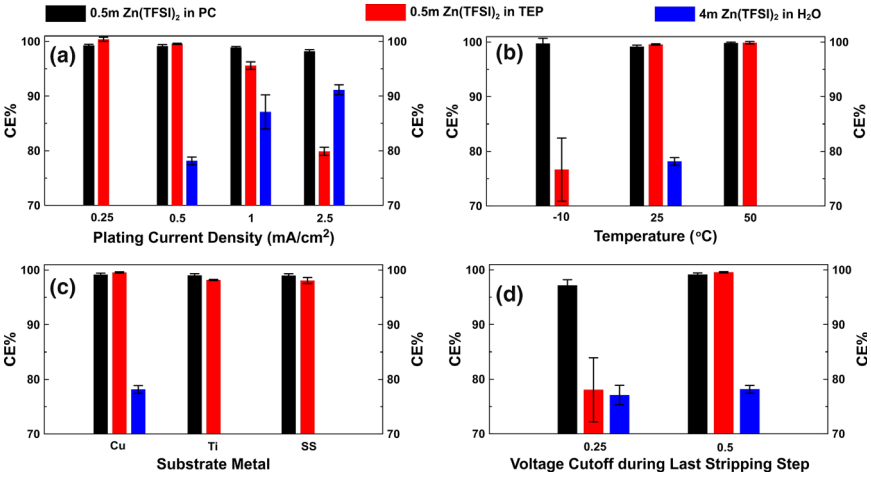

Figure 2. A summary on the effect of different factors: a) current density, b) temperature, c) substrate metal, and d) voltage cutoff during last stripping step on Coulombic efficiency for three representative electrolytes A: 0.5 m Zn(TFSI)$_2$ in PC, B: 0.5 m Zn(TFSI)$_2$ in TEP and C: 4 m Zn(TFSI)$_2$ in H_2O. (a), (b) and (d) refer to Cu substrate.

full cell, we built a three-electrode Swagelok cell including a $Na_2V_6O_{16}{\cdot}1.63H_2O$ (HNVO) working electrode (WE), a Cu counter electrode, and a Zn reference electrode (RE; **Figure 3**a,b). The electrolyte selected for these experiments was 4 m Zn(TFSI)$_2$ in H_2O. Because HNVO was prepared in the "charged" state with no initial capacity, it was first discharged using Zn as the counter electrode at a constant current density of 300 mA g^{-1}, followed by cycling for 2.5 cycles at 25 °C between 0.2 and 1.6 V versus Zn (Figure 3c). The final step ensured the full intercalation of Zn^{2+}/H^+ into HNVO cathode. The discharged HNVO was then connected with Cu as the counter electrode to make a simulated "anode-free" Zn battery, with an auxiliary Zn electrode to provide an accurate reference for potentials of both HNVO (WE or the simulated cathode) and Cu (counter electrode or the simulated anode). After a single charge and discharge step, surprisingly, the final Zn stripping potential (vs Zn/Zn^{2+}) from the Cu anode current collector was only ~0.1 V versus Zn when the HNVO|Zn full cell reached the 0.2 V discharge voltage limit (Figure 3d), which is much lower than most of the reported upper potential limits (e.g., 0.5, 1 V, etc.) adopted for Zn CE protocols. In other words, many reported CE values may not even be close to achievable during practical RZMB operation. The underlying reason why electrolytes with significant voltage polarization (such as electrolyte B) or those with long-term stability issues (such as electrolyte C) yield particularly poor performance in full RZMBs becomes clear: the plated Zn on the anode never reaches a sufficiently high potential to completely strip by the end of discharge. These unrealistic upper voltage limits for Zn stripping in CE measurements are responsible for the pronounced gap between promising CE values and mediocre full cell performance.

By testing Zn electrolytes with a rigorous protocol designed with the ultimate goal of a RZMB in mind, it is possible to establish correlations between electrochemical performance and fundamental electrolyte properties, potentially guiding future electrolyte development. Echoing the work by Amine and co-workers,[29,30] we examined the role of the electrolyte solvent in the kinetics of interfacial charge transfer reactions and the deposition of a passivating interphase on the electrode surface. In the case of lithium-ion batteries or batteries with Li metal anodes, it has been argued that the solvating strength of the electrolyte solvents should be lessened to promote salt aggregation, so that preferential reduction of fluorinated anions can outcompete solvent reduction, leading to an inorganic and dense solid electrolyte interphase (SEI). Consequently, weaker solvation also lowers the charge transfer barrier for ion exchange during plating/stripping (de-solvation/solvation). However, this approach may be inappropriate for Zn^{2+}, as most of the reversibility issues of divalent ion batteries (Mg^+, Ca^+, and Zn^{2+}) center around poor salt solubility in electrolytes and sluggish ion transport through residual oxide and SEI layers. In this regard, a molecular-level understanding afforded by computational chemistry could direct electrolyte design efforts.

Here, we used DFT calculations to predict the relative solvating strength of noteworthy Zn electrolytes through calculation of the bulk solvation free energy of Zn^{2+} and ZnO in TEP, PC, fluoroethylene carbonate (FEC), and 3,3,3-fluoroethylmethyl carbonate (FEMC) using a cluster–continuum approach (CCA). Solvation free energy in the CCA reflects the binding free energy to form a cluster of n-solvent (S_n)

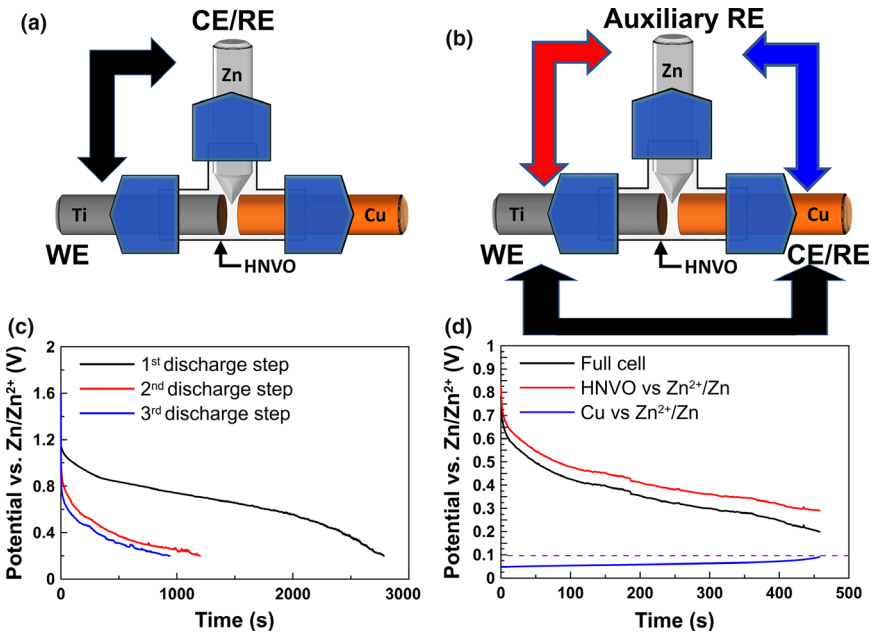

Figure 3. A Swagelok-based three-electrode cell setup for a) HNVO|Zn cell pre-cycling and b) Zn stripping potential testing. Potential versus time for c) the first three discharge process of HNVO|Zn cell (shown in Figure 3a) and d) discharge processes of HNVO|Cu cell (shown in Figure 3b) with a current of 300 mA g^{-1} between 0.2 and 1.6 V at 25 °C. The electrolyte was 4 m $Zn(TFSI)_2$ in H_2O.

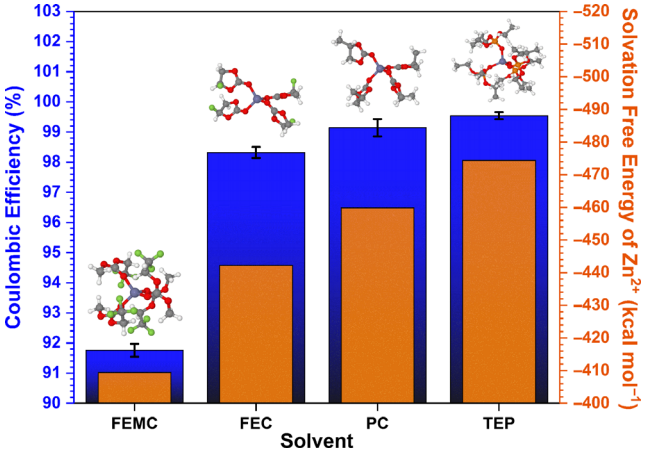

Figure 4. Correlation between measured Coulombic efficiency and solvation free energies of Zn^{2+} solvent tetramers from density functional theory calculations with implicit solvent. Jmol color scheme, visualized with VESTA.[33,34]

molecules with a solute (X) and adds an approximate correction to solvate the XS_n cluster. Despite such calculations lacking the granular treatment of an explicit electrode surface and competitive solvation effects in the inner Helmholtz layer, the results for Zn^{2+} solvation summarized in **Figure 4** highlight the correlation between solvation and CE (measured using the method shown in Figure 1 at 25 °C). Of the solvents considered, FEMC is found to have the lowest solvating strength for Zn^{2+} and undergoes significant solvent reorganization as CF_3 groups are expelled with increasing cluster size. As shown in Figure S13, the order of binding free energies changes as the first Zn^{2+} solvation shell gets filled indicating that simple calculations performed using only one solvent with Zn^{2+} would yield wrong trends compared with calculations considering a full Zn^{2+} solvation shell. There is no clear correlation between voltage polarization shown in Figure S14 and solvation energy indicating that other factors such as SEI resistance, morphology, and surface area of plated Zn significantly contribute to overpotentials during deposition and stripping. Similar Zn^{2+} solvation in PC and TEP indicates similar salt dissociation in these electrolytes resulting in similar conductivities (see Figure S5). Much higher salt aggregation is expected in FEMC.

A consequence of tuning electrolyte solvating strength is the ability to alter the stability or solubility of residual films on the Zn surface, and in situ products generated from solvent and/or anion decompositions. It has been shown previously that relatively simple calculations afford insight into this area as well.[31,32] As a simple example, we consider solvation and/or reactivity of these solvents with ZnO, which is initially present on the anode surface and continues to form during cycling through precipitation of zincates. It is found that TEP has the greatest solvating strength toward ZnO (Figure S15), supported by van der Waals (vdW) interactions between the oxide and ethyl side chains. The $-CH_2-$ from FEMC are also found to support the oxide through favorable vdW interactions, though not to as great of an extent as TEP. In the low dielectric environment near the anode, TEP and FEMC may deprotonate to the oxide (Figure S16a-c) with very low barrier, conditioning the anode surface through conversion of ZnO, possibly to hydroxides. The higher solvating strength of TEP translates to greater solubility of the hydroxides as $Zn(OH)_2$ or zincates and some initial removal of the material from the surface. Despite its reactivity with ZnO, FEMC will have a lower capacity for surface conditioning due to its low solvating strength in comparison to the other solvents. Conversely, PC and FEC are much less likely to participate in the oxide conversion chemistry at all due to a ~3 kcal mol^{-1} solvent reorganization penalty which disfavors the more reactive reverse orientation of one of the carbonate molecules (Figure S16d,e). Thus, modeling suggests that multiple competing mechanisms, such as solvent deprotonation on ZnO followed by decomposition and SEI formation, compete with the solvation of the native passivation film and anode surface conditioning during cycling, as summarized in **Table 1**.

The high solvating strength of TEP also extends to products resulting from anion decomposition, where X-ray photoelectron spectroscopy (XPS) reveals greater ZnF_2 character in the SEI formed in TEP during the first 20 h of cycling when compared to PC, which has greater organic content (Figure S17a,b). After 200 h of cycling (Figure S17c, d), XPS reveals a significant increase in the organic content of the SEI formed in TEP which may contribute to the increasing polarization observed over time. The more mixed organic/inorganic nature of the SEI formed in PC results in a less mechanically robust passivation layer. Decreasing interfacial impedance in PC with cycling (see Figure S6) indicates either dissolution of SEI or surface roughening that ultimately

Table 1. A summary of the factors affecting CE and their relationship to observed behaviors during cycling.

Solvent ⟶	TEP	PC	FEC	FEMC
Salt aggregation	Low	Low	Mod.	High
Solubility of decomp. products	Highest	High	Mod.	Low
Deprotonation to ZnO	Yes	Unlikely	Unlikely	Yes
Composition of SEI (initial)	Inorganic	Org./Inorg.	Org./ Inorg.	Org./ Inorg.
Composition of SEI (final)	Org./Inorg.	Org./Inorg.	Org./ Inorg.	Org./ Inorg.
Voltage polarization	High (increasing)	Low (decreasing)	Low	High
Dendrite growth probability	Low	High	High	Low
Cont. electrolyte decomposition	No	No	No	Yes

Green, yellow, and red text denotes positive, neutral, and negative effects, respectively. CE, Coulombic efficiency; Cont., continuous; Decomp., decomposition; FEC, fluoroethylene carbonate; FEMC, 3,3,3-fluoroethylmethyl carbonate; Inorg., inorganic, ZnF_2; Mod., moderate; Org., organic; PC, propylene carbonate; TEP, triethyl phosphate.

leads to dendrite formation and cell failure (Figure S14b,c). The weaker solvents of FEC and FEMC promote a higher degree of salt aggregation and so are more likely to grow thicker, more heterogeneous organic/inorganic SEIs. The same issues that lead to dendrite and cell failure in PC likely extend to FEC as well. However, the large polarization and lower CE observed for FEMC may be indicative of continuous electrolyte decomposition. Together, these factors suggest careful selection of solvent/salt combinations may promote control over performance aspects beyond CE including polarization, propensity for dendrite growth, and self-discharge rate.

3. Conclusion

In this work, we transplanted an established galvanostatic protocol for CE determination of Li systems to the zinc chemistry and explored how certain critical factors dictate the reversibility of various Zn electrolytes. The initial results suggest that non-aqueous electrolytes generally exhibit more reversible Zn plating/stripping behavior than most of the common aqueous electrolytes, but their ability to support RZMB full cell chemistries is not considered. In an effort to establish a rigorous protocol relevant to practical RZMBs, we tracked the final Zn stripping potential in an HNVO|Zn(Cu) full cell using a Swagelok-based three-electrode setup, and for the first time systematically investigated the impact of an accurate upper cutoff voltage on Zn CE value. Based on these results and complementary DFT calculations, we identified an intrinsic correlation between CE and solvent binding energy, thus connecting solvation behavior of different solvent molecules to the electrochemical performance of Zn metal anodes in corresponding electrolytes. The availability of a standard protocol that can serve as a rapid and precise quantifier for Zn metal reversibility across different electrolyte systems is of utmost importance to the continued development of RZMBs. We hope that this work will encourage informed and rigorous practices that will be adopted as part of future Zn research, so that new advances in this field can be more accurately evaluated against the requirements of a practical Zn metal anode battery.

4. Experimental Section

Electrochemical Characterization: The Cu|Zn, Ti|Zn, SS|Zn, and Zn|Zn cells were assembled in 2032-type coin cell sets using a piece of glass fiber (Whatman GF/F) as separator and various prepared solution as electrolyte (150 µL per cell). All the cells and electrolytes were prepared in Ar filled glovebox. All the charge–discharge testing was conducted at −10, 25, or 50 °C using a Maccor Series 4000 cycler. The CE measurement method follows the protocol for a lithium metal anode reported by Adams et al.[26] (Method 3). Substrate metal (i.e., Cu, Ti and SS) was conditioned by plating (0.5 mA cm^{-2}, 5 mAh cm^{-2}) and stripping Zn (0.5 V) during the first cycle. Then, a Zn reservoir with a capacity of 5 mAh cm^{-2} (Q_t) was built on the substrate metal by using the same current density used for the following cycling. Different current densities (i.e., 0.25, 0.5, 1 and 2.5 mA cm^{-2}) were used for stripping and plating 1 mAh cm^{-2} (Q_c) of Zn during the subsequent nine cycles. In the final step, the recoverable capacity (Q_s) was stripped by charging to a certain voltage (i.e., 0.25, 0.5 V). The average CE is calculated based on the following Equation 1:

$$CE = \frac{9Q_c + Q_s}{9Q_c + Q_t} \quad (1)$$

The Swagelok three-electrode cell setup shown in Figure 3 was used to track the potential of Cu (vs Zn/Zn^{2+}) in an HNVO|Zn(Cu) full cell at the end of discharge. In the setup configuration, the HNVO was the working electrode and the Zn rod acted as both reference electrode and counter electrode. This HNVO|Zn cell was cycled 2.5 times between 0.2 and 1.6 V with a current of 300 mA g^{-1} at room temperature. This cycling finished when the HNVO|Zn cell reached a fully discharged cell voltage of 0.2 V. This initial step served to "activate" the HNVO. In the subsequent test configuration, we kept the HNVO as a working electrode and connected Cu as the counter electrode. This HNVO|Cu cell was then charged to 1.6 V and discharged to 0.2 V. As part of this procedure, the Zn rod acted as a reference electrode for HNVO and Cu, respectively, to track their potential change during this process. To confirm the integrity of this Zn reference (since it was previously cycled during HNVO activation), a similar Swagelok three-electrode cell setup (with pristine Zn reference electrode) was also used to prove the stability of Zn electrode after formation cycle above (Figure S12). A Modulab XM ECS (Solartron Analytical) was the instrument used for this measurement.

Zn|Zn symmetric cells were cycled using 0.5 mA cm^{-2} at room temperature. Each half cycle (charge or discharge) was set to 1 h.

Electrochemical impedance spectroscopy (EIS) measurements were conducted on Zn|Zn symmetric cells with 0.5 m $Zn(TFSI)_2$ in PC or 0.5 m $Zn(TFSI)_2$ in TEP before or after 20 and 200 h cycling at zero state of charge at 25 °C (0.5 mA cm^{-2}, 0.5 mAh cm^{-2}). Alternating current (AC) impedance spectra were collected with ten points per decade from 100 kHz to 10 mHz with a signal amplitude of 10 mV at 25 °C. A single-channel Gamry Potentiostat (Reference 3000) was used for data collection.

Ionic conductivities of the electrolytes were determined from impedance scans from 20 Hz to 2 MHz with an amplitude of 20 mV using

an Agilent E4980A precision LCR meter. The conductivity cell was adapted from a YSI 3418 cell to make it fit tightly into a polyethylene bottle for holding an electrolyte. The cell constant (0.1 cm^{-1} nominal) was calibrated with a 100 mS cm^{-1} standard solution. Temperature of the sample cell, along with a reference cell, was ramped down from 60 to −20 °C then back up at 0.1 °C min^{-1} in a Tenney Jr. Environmental Chamber while the impedance was continuously scanned. A thermocouple was each attached to the sample and reference cells, and the temperature difference was recorded for the phase changes of an electrolyte in relation to its changes of conductivity.

X-ray photoelectron spectroscopy measurements (PHI Versaprobe III) were conducted on Zn electrodes obtained by opening coin cells in an argon-filled glovebox, rinsed with anhydrous dimethoxyethane (DME) and dried in an antechamber under vacuum overnight. To avoid the disturbance from air/moisture, the samples were transferred into XPS system using a sealed vacuum transfer capsule. The data were collected by using a combination of survey scan (pass energy 224 eV, step size 1 eV) and high-resolution scan (pass energy 26 eV, step size 0.05 eV). The X-ray was focused to a spot size of 100 μm and had a power of 25 W. Surface neutralization was performed through a combination of a low energy Ar-ion flow with an electron neutralizer, operating pressures were maintained $<6 \times 10^{-6}$ Pa. Peak fitting was performed using PHI's Multipak software v. 9.6, using 70/30 Gaussian/Lorentzian line shapes on a Shirley background. All spectra were shifted relative to the binding energy of the carbon 1s sp3 (assigned to 284.8 eV) to compensate for any surface charging off-set during the measurement.

Acknowledgements

This work was supported by the Joint Center for Energy Storage Research (JCESR), a Department of Energy, Energy Innovation Hub, under an Interagency Agreement No. IAA SN2020957. One of the authors (LM) also wants to acknowledge the financial support from the Dr. Brad. E. Forch Distinguished Postdoctoral Fellowship administered by the National Research Council as well as prior support from Oak Ridge Associated Universities (ORAU). Dr. Jeff Read (ARL) and Dr. Yue Li (UMD) provided assistances during the preparation and characterization of the pure Zn salts.

Conflict of Interest

The authors declare no conflict of interest.

Supporting Information

Supporting Information is available from the Wiley Online Library or from the author.

Keywords

Coulombic efficiency, rigorous protocol, Zn ion solvation, Zn metal anode

Received: March 11, 2020
Revised: April 3, 2020
Published online: March 12, 2020

[1] M. Winter, B. Barnett, K. Xu, *Chem. Rev.* **2018**, *118*, 11433.
[2] K. Xu, *Energy Environ. Mater.* **2019**, *2*, 229.
[3] "Abundance of elements in Earth's crust", https://en.wikipedia.org/wiki/Abundance_of_elements_in_Earth%27s_crust (accessed: March 2020).
[4] F. Wang, O. Borodin, T. Gao, X. Fan, W. Sun, F. Han, A. Faraone, J. A. Dura, K. Xu, C. Wang, *Nat. Mater.* **2018**, *17*, 543.
[5] L. Wang, Y. Zhang, H. Hu, H.-Y. Shi, Y. Song, D. Guo, X.-X. Liu, X. Sun, *ACS Appl. Mater. Interfaces* **2019**, *11*, 42000.
[6] C. Zhang, J. Holoubek, X. Wu, A. Daniyar, L. Zhu, C. Chen, D. P. Leonard, I. A. Rodríguez-Pérez, J.-X. Jiang, C. Fang, X. Ji, *Chem. Commun.* **2018**, *54*, 14097.
[7] N. Zhang, F. Cheng, Y. Liu, Q. Zhao, K. Lei, C. Chen, X. Liu, J. Chen, *J. Am. Chem. Soc.* **2016**, *138*, 12894.
[8] H. Li, L. Ma, C. Han, Z. Wang, Z. Liu, Z. Tang, C. Zhi, *Nano Energy* **2019**, *62*, 550.
[9] B. Tang, L. Shan, S. Liang, J. Zhou, *Energy Environ. Sci.* **2019**, *12*, 3288.
[10] K. Kordesch, J. Gsellmann, M. Peri, K. Tomantschger, R. Chemelli, *Electrochim. Acta* **1981**, *26*, 1495.
[11] M. Minakshi, D. Appadoo, D. E. Martin, *Electrochem. Solid-State Lett.* **2010**, *13*, A77.
[12] A. R. Mainar, O. Leonet, M. Bengoechea, I. Boyano, I. de Meatza, A. Kvasha, A. Guerfi, J. Alberto Blázquez, *Int. J. Energy Res.* **2016**, *40*, 1032.
[13] J. F. Parker, C. N. Chervin, I. R. Pala, M. Machler, M. F. Burz, J. W. Long, D. R. Rolison, *Science* **2017**, *356*, 415.
[14] B. J. Hopkins, M. B. Sassin, C. N. Chervin, P. A. DeSario, J. F. Parker, J. W. Long, D. R. Rolison, *Energy Storage Mater.* **2020**, *27*, 370.
[15] S. Higashi, S. W. Lee, J. S. Lee, K. Takechi, Y. Cui, *Nat. Commun.* **2016**, *7*, 11801.
[16] P. He, M. Yan, G. Zhang, R. Sun, L. Chen, Q. An, L. Mai, *Adv. Energy Mater.* **2017**, *7*, 1601920.
[17] H. Pan, Y. Shao, P. Yan, Y. Cheng, K. S. Han, Z. Nie, C. Wang, J. Yang, X. Li, P. Bhattacharya, K. T. Mueller, J. Liu, *Nat. Energy* **2016**, *1*, 16039.
[18] Z. Li, S. Ganapathy, Y. Xu, Z. Zhou, M. Sarilar, M. Wagemaker, *Adv. Energy Mater.* **2019**, *9*, 1900237.
[19] H. Pan, J. F. Ellis, X. Li, Z. Nie, H. J. Chang, D. Reed, *ACS Appl. Mater. Interfaces* **2019**, *11*, 37524.
[20] S. Huang, J. Zhu, J. Tian, Z. Niu, *Chem. Eur. J.* **2019**, *25*, 14480.
[21] N. Zhang, F. Cheng, J. Liu, L. Wang, X. Long, X. Liu, F. Li, J. Chen, *Nat. Commun.* **2017**, *8*, 405.
[22] S.-D. Han, N. N. Rajput, X. Qu, B. Pan, M. He, M. S. Ferrandon, C. Liao, K. A. Persson, A. K. Burrell, *ACS Appl. Mater. Interfaces* **2016**, *8*, 3021.
[23] A. Naveed, H. Yang, J. Yang, Y. Nuli, J. Wang, *Angew. Chemie Int. Ed.* **2019**, *58*, 2760.
[24] A. J. Smith, J. C. Burns, S. Trussler, J. R. Dahn, *J. Electrochem. Soc.* **2010**, *157*, A196.
[25] T. M. Bond, J. C. Burns, D. A. Stevens, H. M. Dahn, J. R. Dahn, *J. Electrochem. Soc.* **2013**, *160*, A521.
[26] B. D. Adams, J. Zheng, X. Ren, W. Xu, J.-G. Zhang, *Adv. Energy Mater.* **2018**, *8*, 1702097.
[27] J. C. Burns, A. Kassam, N. N. Sinha, L. E. Downie, L. Solnickova, B. M. Way, J. R. Dahn, *J. Electrochem. Soc.* **2013**, *160*, A1451.
[28] X. Wei, D. Desai, G. G. Yadav, D. E. Turney, A. Couzis, S. Banerjee, *Electrochim. Acta* **2016**, *212*, 603.
[29] C.-C. Su, M. He, R. Amine, T. Rojas, L. Cheng, A. T. Ngo, K. Amine, *Energy Environ. Sci.* **2019**, *12*, 1249.
[30] M. Li, J. Lu, X. Ji, Y. Li, Y. Shao, Z. Chen, C. Zhong, K. Amine, *Nat. Rev. Mater.* **2020**, 1.
[31] V. S. Bryantsev, *Theor. Chem. Acc.* **2012**, *131*, 1250.
[32] V. S. Bryantsev, M. S. Diallo, W. A. Goddard III, *J. Phys. Chem. B* **2008**, *112*, 9709.
[33] K. Momma, F. Izumi, IUCr, *J. Appl. Crystallogr.* **2011**, *44*, 1272.
[34] R. M. Hanson, IUCr, *J. Appl. Crystallogr.* **2010**, *43*, 1250.

